J. Astrophys. Astr. (2006) **27,** 243–254

Coronal Mass Ejections of Solar Cycle 23

Nat Gopalswamy
NASA Goddard Space Flight Center, Greenbelt, MD 20771, USA.
e-mail: gopals@ssedmail.gsfc.nasa.gov

Abstract. I summarize the statistical, physical, and morphological properties of coronal mass ejections (CMEs) of solar cycle 23, as observed by the Solar and Heliospheric Observatory (SOHO) mission. The SOHO data is by far the most extensive data, which made it possible to fully establish the properties of CMEs as a phenomenon of utmost importance to Sun–Earth connection as well as to the heliosphere. I also discuss various subsets of CMEs that are of primary importance for their impact on Earth.

Key words. Sun: coronal mass ejections, shocks, magnetic field.

1. Introduction

Coronal mass ejections (CMEs), as we know them today, were first detected in the coronagraph images obtained on December 14, 1971 by NASA's OSO-7 spacecraft (Tousey 1973). Typical coronagraphs have an occulting disk to artificially eclipse the bright photosphere, so the faint coronal structures outside the periphery of the occulting disk can be viewed in the photospheric light scattered off these structures. CMEs are now understood as large-scale magnetized plasma structures originating from closed magnetic field regions on the Sun: active regions, filament regions, active region complexes and trans-equatorial interconnecting regions. Definite inferences on mass ejections in the solar atmosphere predated the white-light discovery by decades: prominence eruptions (Secchi and de la Rue in the late 1800s (see, e.g., Tandberg-Hanssen 1995)), slow-drifting radio bursts (Payne-Scott *et al.* 1947), and moving type IV radio bursts (Boischot 1957). There were also other indications around the time of the white light detection: rapid decay of transient coronal condensation (Hansen *et al.* 1971), coronal green line transients (DeMastus *et al.* 1973), helium abundance enhancements in the high speed plasmas behind interplanetary (IP) shocks (Hirshberg *et al.* 1972) later recognized as the IP counterpart of CMEs (Borrini *et al.* 1982). CMEs also existed conceptually as agents causing geomagnetic storms (Lindemann 1919) and driving IP shocks (Gold 1955). A list of review articles covering the three decades of CME research can be found in Gopalswamy (2004). Here, I highlight the recent research on CMEs spurred by the extensive and uniform data from the Solar and Heliospheric Observatory (SOHO) mission's Large Angle and Spectrometric Coronagraph (LASCO, Brueckner *et al.* 1995).

2. CME properties

The basic attributes of a CME are its speed, width, acceleration, and central position angle (CPA), all with reference to the sky plane. These are obtained from a time sequence of coronagraphic images, in which the CME can be recognized as a moving feature occupying a well-defined region. The angular extent of the moving feature defines the width. The central angle of this extent with reference to the solar north is the CPA. The speed is normally determined from a linear fit to the height–time (h–t) plots. But CMEs often have finite acceleration, so the linear-fit speed should be understood as the average value within the coronagraphic field of view. Quadratic fit to the h–t plots gives the constant acceleration, which again is an approximation because the acceleration may also change with time.

The measured sky-plane speed ranges from a few km s^{-1} to $\sim$3000 km s^{-1} (see e.g., Gopalswamy 2004; Yashiro *et al.* 2004), with an average value of $\sim$483 km s^{-1}. The CME speed has a lognormal distribution (Yurchyshyn *et al.* 2005). The apparent angular width of CMEs ranges from a few degrees to more than 120 degrees, with an average value of $\sim$46 deg. The average width was computed for CMEs with width $\leq$120 deg. The true width of halo CMEs (Howard *et al.* 1982), which appear to surround the occulting disk, is unknown. Most of the h-t plots fall into three types: accelerating, constant speed, and decelerating, indicating different degrees of propelling and retarding forces acting on CMEs (Gopalswamy *et al.* 2001a). Figure 1 shows a scatter plot between the measured acceleration (a in ms^{-2}) and speed (v in km s^{-1}) of all the CMEs for which the acceleration estimate was possible. Despite the large scatter, the acceleration has a reasonable correlation with speed: $a = -0.0133(v - 452)$, which shows that slow CMEs ($v < 450$ km s^{-1}) accelerate, CMEs of intermediate speed ($v \sim 450$ km s^{-1}) have no appreciable acceleration, and fast CMEs ($v > 450$ km s^{-1}) decelerate. Close to the Sun, a is determined by the propelling force, gravity and coronal drag. Note that $a = 0$ for $v = 452$ km s^{-1} means that the solar wind has already picked up speed within the LASCO field of view. The CME acceleration over the entire Sun–Earth distance also has a similar relation to the CME initial speed (Gopalswamy *et al.* 2001b): $a = -0.0054\ (v - 406)$. In this case, the propelling force and gravity become less important and the drag force dominates so that $v = 406$ km s^{-1} corresponds to the average solar wind speed.

The width is a good indicator of the mass content of CMEs. The mass is estimated as the excess mass in the coronagraphic field of view assuming that the entire mass is located in the sky plane (see, e.g., Vourlidas *et al.* 2002). Like the width, the mass also changes during the early phase of the CME before stabilizing to a near-constant value. This constant value is used as the representative mass. Figure 2 shows that the mass ranges from a few times 10^{13} g to more than 10^{16} g. The kinetic energy obtained from the measured speed and mass ranges from $\sim 10^{27}$ erg to $\sim 10^{32}$ erg, with an average value of 5×10^{29} erg. Some very fast and wide CMEs have kinetic energies exceeding 10^{33} erg, generally originating from large active regions [Gopalswamy *et al.* 2005a]. Most of these results are similar to those obtained by pre-SOHO coronagraphs, except for the smaller average mass and a larger number of fast and wide CMEs, including halo CMEs.

CMEs often display spatial structures, commonly referred to as the 'three-part structure' (a frontal structure, central bright core, and cavity – see Hundhausen 1999). The frontal structure overlies the cavity, which contains the bright core. The core has been

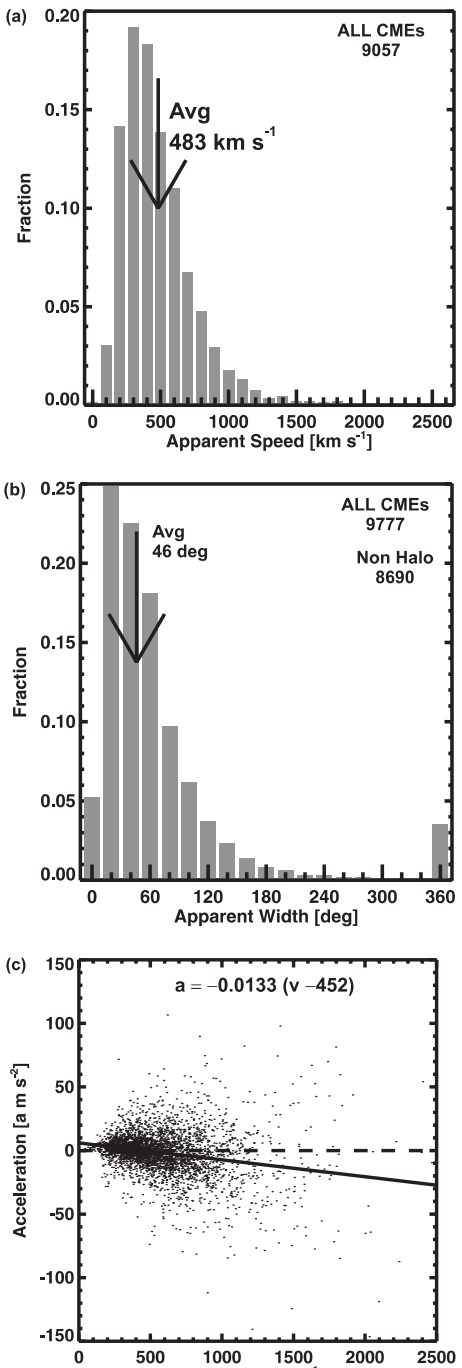

Figure 1. CME speed **(a)**, width **(b)** and acceleration **(c)** of all CMEs from 1996 to June 2005. The acceleration has a large scatter, but there is a clear trend that the fast CMEs decelerate, while slow CMEs accelerate.

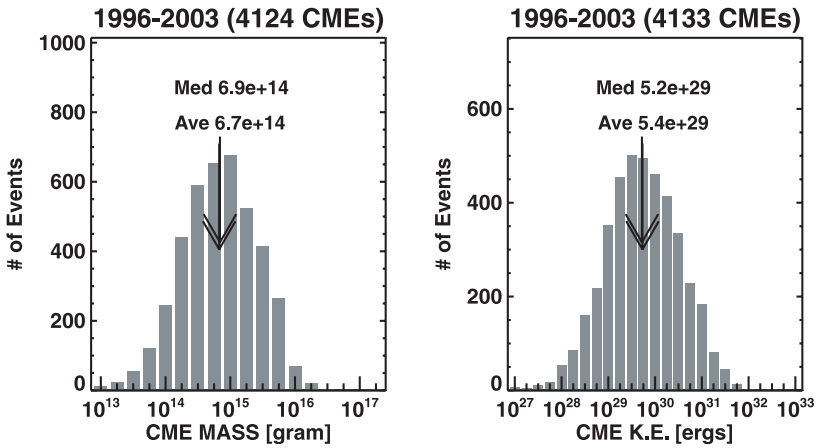

Figure 2. CME mass (left), and kinetic energy (right) of SOHO CMEs for the period 1996–2003.

shown to be the eruptive prominence by comparing coronagraph and H-alpha observations. Eclipse pictures often show the three-part structure in the pre-eruptive stage, where the helmet streamer takes the place of the frontal structure. Not all CMEs show the three-part structure either due to geometrical reasons (Cremades *et al.* 2004) or due to the nature of the source region. Halo CMEs often contain a diffuse front with a bright inner feature of smaller spatial extent. The cavity, if any, must have been obscured by the overlying structure. If the CME is fast with respect to the local Alfvén speed, it drives a shock. Such CMEs must have four-part structure, but the shock is often difficult to detect. The circular shape of the outermost structure in halo CMEs may indeed be a manifestation of the shock (Sheeley *et al.* 1999).

The CME plasma is multithermal with the prominence core at $\sim$8000 K and the outer structure at a few MK. Occasionally, CMEs may consist of flare ejecta with temperature exceeding 10 MK. The magnetic field in CMEs is not directly measurable near the Sun. The magnetic field in prominences is typically up to 30 G, while it can exceed 1000 G in the active region cores. The field strength in the outer corona is typically less than $\sim$1 G. The coronal cavity overlying the filament may also have field strengths higher than the overlying corona for pressure balance requirements. The 1-AU field strength in CMEs is typically tens of nT, which is up to an order of magnitude higher than the field in the quiet solar wind (a few nT). Tens of nT at 1 AU correspond to tens of G at the Sun if we assume a simple r^{-2} dependence. This is consistent with the field strength in the prominence and the inferred values in the overlying coronal cavity.

3. CME rate and implications

How frequently do CMEs occur? During solar minima, one CME occurs every other day. The rate goes up to several per day during solar maximum. On one day during solar maximum, 13 CMEs were recorded by SOHO; there were several days with more than 10 CMEs (Gopalswamy *et al.* 2003a). The daily CME rate averaged over Carrington Rotations (27.3 days) was found to exceed 6/day (see Fig. 3). During cycle 23, the rate

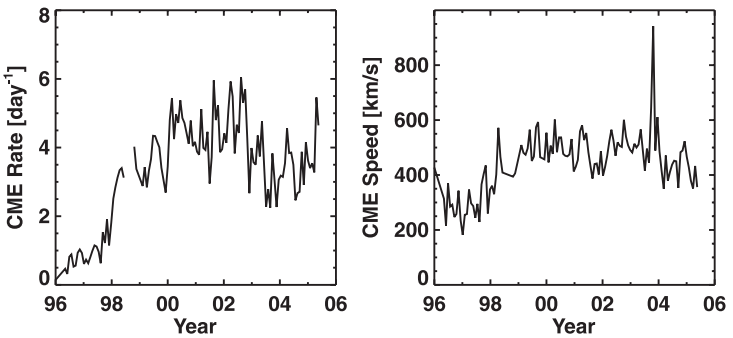

Figure 3. CME rate (left) and mean speed (right) averaged over Carrington Rotation (CR) periods. The gap in the CME rate is due to the temporary disability of SOHO during June–October 1998. The large spike in the CME mean speed is due to the Halloween 2003 CMEs.

increased abruptly in 1998 and remained relatively high through the middle of 2002. There is a general decline after 2002, but the rate is still much higher than the solar minimum values (as of mid 2005). The large spikes in Fig. 3 are due to superactive regions, which are prolific producers of CMEs.

The pre-SOHO CME rate was found to have a good correlation with the sunspot number (SSN), which indicated a solar maximum rate of $\sim$3 (Hildner *et al.* 1976), confirmed by data from the SMM and Solwind coronagraphs (Cliver *et al.* 1994). The SOHO CME rate, although initially consistent with pre-SOHO results (St Cyr *et al.* 2000), has several unexpected aspects:

- The solar maximum rate nearly doubled to 6/day.
- While SOHO data confirmed the SSN-CME rate relationship, the correlation is less than perfect, which can be attributed to the high-latitude (HL) CMEs associated with the polar crown filaments (PCFs) around solar maximum. The HL CMEs are not associated with sunspots (Gopalswamy *et al.* 2003a,b) and hence the weaker correlation.
- The SSN and CME rate reached maximum at different peaks of the double maximum (late 2000 for SSN and mid 2002 for CME rate). This result also follows from the fact that the HL CMEs are associated with PCF (spotless eruptions), while the low-latitude (LL) CMEs are predominantly from sunspot regions (except for some CMEs associated with low-latitude quiescent prominences).
- There is a remarkable coincidence between the cessation of HL CMEs and the polarity reversal at solar poles. This result holds good for individual poles, which reversed at different times (north in July 2000 and south in May 2002) (Gopalswamy *et al.* 2003b).
- The rate of CMEs and the minimum-to-maximum variability, originally thought to be inadequate (Newkirk *et al.* 1981; Wagner 1984), have been found to be large enough to cause galactic cosmic ray modulation (Gopalswamy 2004; Lara *et al.* 2005). HL CMEs have been found to be more effective in suppressing the cosmic rays during the $A > 0$ epoch (when solar north pole has north polarity), while the LL CMEs seem to be dominant in the $A < 0$ epoch (when solar north pole has south polarity). The galactic cosmic rays enter the heliosphere from the polar

regions during the A > 0 epochs (encountering HL CMEs on their path), while they enter in the equatorial region during the A < 0 epochs (encountering the LL CMEs).

Another CME attribute linked with solar activity is the mean speed, which doubled from minimum to maximum. This was not firmly established during cycle 22 (Webb & Howard 1994; Hundhausen 1999; Gopalswamy *et al.* 2003a). The mean speed also shows the double peak but the difference between the first and second peaks is not significant. The huge spike in the mean speed is due to the famous Halloween events (October–November 2003) when an extraordinary set of fast CMEs occurred from three active regions (AR 10484, 10486, and 10488) that had significant consequences throughout the heliosphere (see Gopalswamy *et al.* 2005b for a list of publications on these events).

4. CMEs and space weather

CMEs are large-scale magnetized plasma structures, so their propagation into the heliosphere has important consequences. Earth-directed CMEs are likely to impact the magnetosphere to cause geomagnetic storms. CME-driven shocks accelerate solar energetic particles (SEPs). Gosling (1993) had pointed out the central role played by CMEs in causing intense geomagnetic storms. This became further clear when the direct connection between CMEs and their interplanetary counterparts (ICMEs) was established (Burlaga 1981; Lindsay *et al.* 1999; Gopalswamy *et al.* 2000). Halo CMEs, once thought to be of questionable existence, have proved to be the major players in space weather, thanks to the high sensitivity and large field of view of the SOHO/LASCO coronagraphs (see, e.g., Webb *et al.*, 2000). The geoimpact of CMEs generally falls into two categories: geoeffectiveness and SEPeffectiveness. Geoeffective CMEs cause non-recurrent (also known as transient) geomagnetic storms. SEP-effective CMEs cause the gradual and long-lasting SEP events with an intensity of at least 10 pfu in the >10 MeV channels of particle detectors such as on GOES.

4.1 *Geoeffective CMEs*

CMEs originating from close to the disk center (most of which become front-side halos) directly impact Earth and produce geomagnetic storms provided their magnetic field has a southward component (Bs). The impact is marked by the sudden commencement if the CME drives a shock. If the shock sheath region has a Bs, the storm starts immediately after the shock. ICMEs with a flux rope structure (magnetic cloud), almost always cause a storm because either the front or the rear section of the ICME contains Bs. Occasionally CMEs arrive at Earth with a high inclination resulting in an intense storm (when the magnetic field is fully southward, see Gopalswamy *et al.* 2005c) or no storm at all (when the magnetic field is fully northward, see Yurchyshyn *et al.* 2001). The CME speed and the strength of the magnetic field it contains primarily decide the intensity of the geomagnetic storms: Figure 4 shows that the product of CME speed (Vcme) and the 1-AU field strength (B) has the best correlation with Dst index. Various combinations Vcme, ICME speed (Vmc), B, and Bs have been considered in the past (Yurchyshyn *et al.* 2004; Srivastava & Venkatakrishnan 2004 and references therein), but most of the correlation coefficients are generally lower than the one given

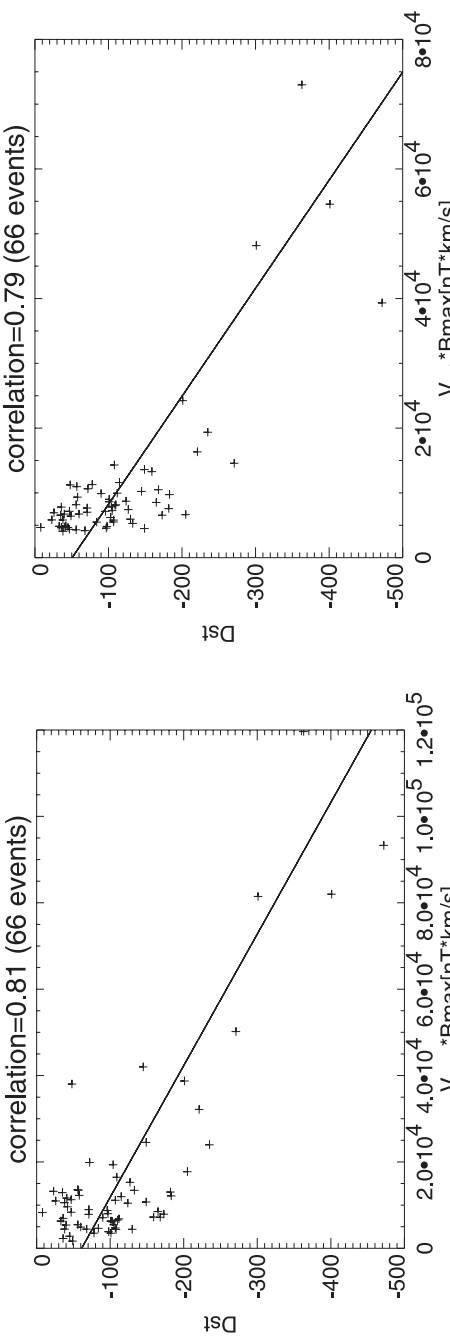

Figure 4. Correlation VcmeB (left) and VmcB (right) with Dst (nT), where B is the 1-AU magnetic field in CMEs, Vcme is the CME speed near the Sun and Vmc is the speed of the magnetic clouds at 1 AU. The suffix "max" indicates the peak value measured at 1 AU.

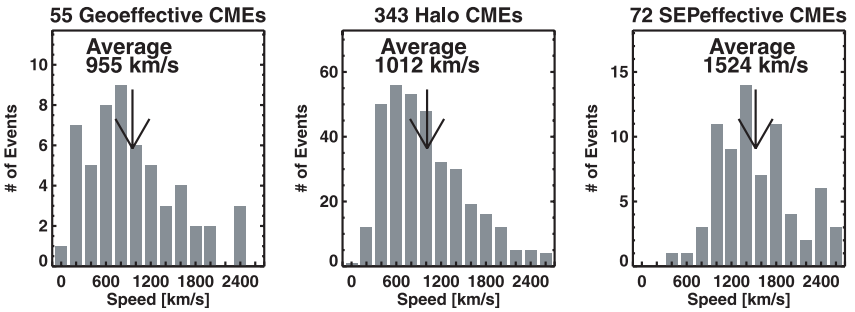

Figure 5. Speed distributions of geoeffective CMEs (left), Halo CMEs (middle) and SEPeffective CMEs (right). The mean speeds are marked.

in Fig. 4. Of course, the best set of parameters will be Vcme and the CME magnetic field (Bcme) measured near the Sun. We are far from obtaining Bcme, so we used the 1-AU B as proxy.

4.2 *SEPeffective CMEs*

The gradual SEP events are thought to originate from CME-driven shocks (Reames 1999; Kahler 2001; Gopalswamy *et al.* 2003c; 2004). The associated CMEs are fast and wide (average speed ~ 1500 km s^{-1}, mostly full or partial halos – see Fig. 5). SEP events with ground level enhancements (GLEs) are associated with the fastest of all CMEs (average speed ~ 2000 km s^{-1}, see Gopalswamy *et al.* 2005d). Up to 15% of the CME kinetic energy goes into the accelerated particles (Emslie *et al.* 2004), suggesting that the CME-driven shocks are efficient particle accelerators. The SEP events are also closely related to type II radio bursts (Gopalswamy 2003; Cliver *et al.* 2004) since the same shocks accelerate SEPs and electrons. There is also a hierarchical relationship between type II bursts and CME kinetic energy (Gopalswamy *et al.* 2005e): CMEs with above-average kinetic energy produce type II bursts confined to the metric (m) domain; CMEs with moderately high kinetic energy produce type II bursts in the decameter-hectometric (DH) domain; CMEs with the highest kinetic energy produce type II bursts over all the wavelength domains (metric to kilometric or mkm). There is also a small population of purely km type II bursts due to accelerating CMEs that drive shocks only at large distances from the Sun. It is not surprising that most of the CMEs associated with mkm type II bursts are also associated with SEP events (see also Fig. 6).

4.3 *Comparing geoeffective and SEPeffective CMEs*

Figure 5 compares the speeds of geoeffective CMEs, halo CMEs, and SEPeffective CMEs. Clearly the halo and geoeffective CMEs have the same average speed, as expected. The SEPeffective CMEs, on the other hand, are much faster. One might wonder why the number of geoeffective CMEs is only $\sim 1/6$ of the number of halos. First of all, only $\sim$half of the halos are front-sided. Only about a third of the front-side halos are likely to originate within 30 deg. of the disk center and this number is

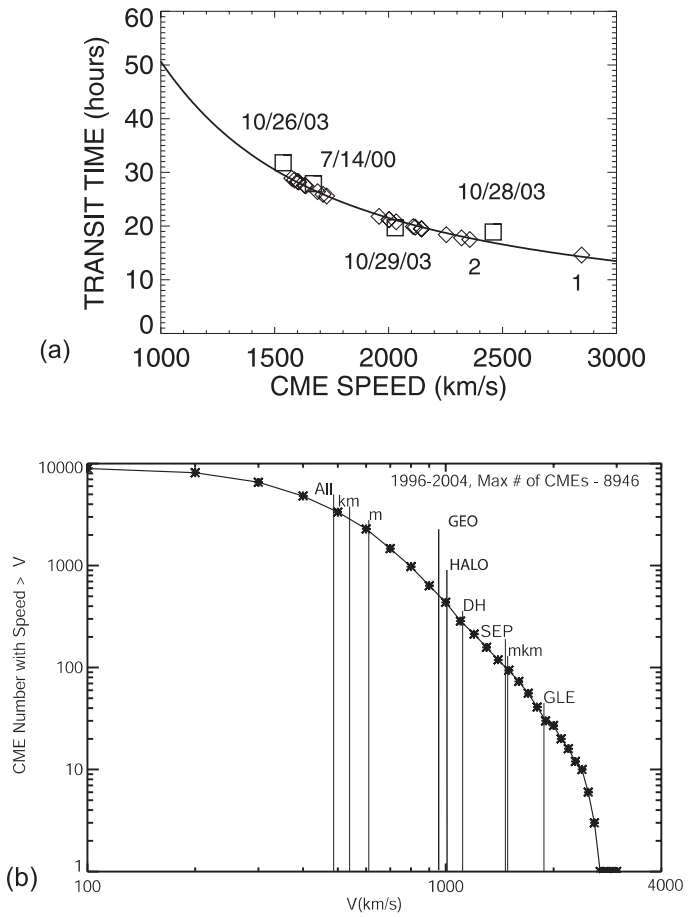

Figure 6. **(a)** The Sun–Earth transit time of CME-driven shocks according to the ESA model approximates as $T = ab^V + c$, where $a = 151.002, b = 0.998625$, and $c = 11.5981$ (solid curve). The open squares are fast-transit events of cycle 23. The diamonds are the historical events, with the two fastest events marked: (1) August 4, 1972 and (2) September 1, 1859. **(b)** The number of CMEs above a certain speed, V (cumulative lognormal distribution) with the average speeds of various CME populations marked.

similar to the number of geoeffective CMEs. Most of the false alarms are caused by asymmetric halos (which originate beyond 30 deg from disk center). Another cause may be merging between successive CMEs. The source regions of the SEPeffective CMEs are generally located on the western hemisphere, although occasionally they do originate from the eastern hemisphere (Gopalswamy *et al.* 2005). The geoeffective CMEs, on the other hand, originate close to the disk center. Thus, the union of SEP- and geoeffective CMEs (most of the front-sided fast and wide CMEs) is important in deciding the conditions in Earth's space environment; their intersection defines the set of CMEs having multiple effects (producing both SEP events and geomagnetic storms).

4.4 *Sun–Earth transit of geoeffective CMEs*

The speed distribution of the geoeffective CMEs gives an indication of the time taken by the CME-driven shocks to arrive at Earth. Figure 6 (left) shows the travel time of shocks driven by CMEs with speeds $\geq 1000\,\mathrm{km\,s^{-1}}$. The solid curve is the empirical shock arrival (ESA) model, which relates the Sun–Earth transit time (T in hours) to the CME speed ($V\,\mathrm{km\,s^{-1}}$) by the formula, $T = ab^V + c$, where $a = 151.002$, $b = 0.998625$, and $c = 11.5981$ (Gopalswamy *et al.* 2005a). T ranges from 50 h for $1000\,\mathrm{km\,s^{-1}}$ CMEs to 13.5 h for $3000\,\mathrm{km\,s^{-1}}$ CMEs. Also shown are some fast-transit shocks from SOHO (the Bastille Day shock of 2000 and three shocks from the Halloween 2003 period). The transit times of historical fast-transit events, whose CME speeds are inferred from the above formula, are also shown for comparison. The transit-time formula suggests that the Sun–Earth transit times of shocks may not exceed ~ 12 h, because the number of CMEs with speeds exceeding $2500\,\mathrm{km\,s^{-1}}$ drops precipitously (see the cumulative distribution shown in Fig. 6).

In summary, we need to worry only about a subset of CMEs for space weather purposes:

- CMEs associated with DH and mkm type II bursts,
- SEP-producing CMEs,
- geoeffective (or halo) CMEs. Figure 6 (right) shows that there are only ~ 1000 CMEs ($\sim 10\%$ of all CMEs) that fall into this group. CMEs associated with SEPs having ground level enhancement (GLE) have the largest speed, while the CMEs associated with purely metric (m) and purely kilometric (km) type II bursts have just above average speeds.

5. Concluding remarks

The high quality data over an extended period of time from SOHO have provided new insights into the problem of CMEs. We now recognize that CMEs constitute the most energetic phenomenon in the heliosphere. While we have a good idea on the kinematic properties of CMEs, their magnetic properties, especially close to Sun, are poorly understood. It is ironic that the magnetic properties are primary indicators of CMEs at 1 AU, but near the Sun, there is very limited information. Understanding the vector magnetic fields of CMEs near the Sun, and their relation to surface and subsurface evolution is crucial in developing long-term prediction of CME production. This will also aid the prediction of potential geoimpact because the magnetic field orientation is a critical parameter. We have seen that only the fast and wide CMEs ($\sim 10\%$ of all the CMEs) have space weather implications. Therefore, modeling efforts should concentrate on these CMEs for space weather applications. SOHO has provided a great deal of information on the initiation and 3D structure of CMEs. Yet, connecting disk signatures to coronagraphic signatures is still not easy due to the occulting disk employed by the coronagraphs. The STEREO mission is likely to alleviate some of these difficulties. STEREO has also the capability to provide information on the early-phase acceleration of CMEs. While the connection between SEP events and CMEs is fairly clear, there are many fast and wide CMEs that are not associated with SEPs. This needs a better characterization of the ambient medium such as density and magnetic field, which determine the local Alfvén speed and hence shock formation. The effects

of CME-induced turbulence and successive CMEs in the ambient medium have to be incorporated into the shock-acceleration theories.

Acknowledgements

I thank S. Yashiro for help with figures. This work was supported by NASA's SR & T and LWS programs.

References

Boischot, A. 1957, *Comptes Rendus Acad. Sci.*, **244**, 1326.
Borrini, G., Gosling, J. T., Bame, S. J., Feldman, W. C. 1982, *J. Geophys. Res.*, **87**, 4365.
Brueckner, G. E. *et al.* 1995, *Solar Phys.*, **162**, 357.
Burlaga, L., Sittler, E., Mariani, F., Schwenn, R. 1981, *J. Geophys. Res.*, **86**, 6673.
Cliver, E. W., St. Cyr, O. C., Howard, R. A., McIntosh, P. S. 1994, In: *Solar coronal structures*, Rusin, V., Heinzel, P., Vial, J.-C., (eds) page 83, VEDA Publishing House of the Slovak Academy of Sciences.
Cliver, E. W., Kahler, S. W., Reames, D. V. 2004, *ApJ*, **605**, 902.
Cremades, H., Bothmer, V. 2004, *Astron. Astrophys.*, **422**, 307.
DeMastus, H. L., Wagner, W. J., Robinson, R. D. 1973, *Solar Phys.*, **31**, 449.
Emslie, A.G. *et al.* 2004, Energy partition in two solar flare/CME events, *J. Geophys. Res.*, **109**, A10104, doi:10.1029/2004JA010571.
Gold, T. 1955, In :*Gas Dynamics of Cosmic Clouds* (eds) van de Hulst, H. C., Burgers, J. M., North-Holland, Amsterdam, p. 103.
Gopalswamy, N. 2003, *Geophys. Res. Lett.*, **30(12)**, SEP 1–1.
Gopalswamy, N. 2004, In: *The Sun and the Heliosphere as an Integrated system* (eds) Poletto, G., Suess, S., Kluwer, Boston, p. 201.
Gopalswamy, N. *et al.* 2000, *Geophys. Res. Lett.*, **27**, 145.
Gopalswamy, N. *et al.* 2001a, *J. Geophys. Res.*, **106**, 29219.
Gopalswamy, N. *et al.* 2001b, *J. Geophys. Res.*, **106**, 29207.
Gopalswamy, N., Lara, A., Yashiro, S., Nunes, S., Howard, R. A. 2003a, In: *Solar variability as an input to the Earth's environment* (ed.) Wilson, A., ESA Publications Division, Noordwijk, p. 403.
Gopalswamy, N., Lara, A., Yashiro, S., Howard, R. A. 2003b, *ApJ*, **598**, L63.
Gopalswamy, N. *et al.* 2003c, *Geophys. Res. Lett.*, **30(12)**, SEP 3–1.
Gopalswamy, N., Yashiro, S., Krucker, S., Stenborg, G., Howard, R. A. 2004, *J. Geophys. Res.*, **109**, 12105.
Gopalswamy, N., Yashiro, S., Liu, Y., Michalek, G., Vourlidas, A., Kaiser, M. L., Howard, R. A. 2005a, *J. Geophys. Res.*, **110**, A09S15, doi:10.1029/2004JA010958.
Gopalswamy, N., Barbieri, L., Cliver, E. W., Lu, G., Plunkett, S. P., Skoug, R. M. 2005b, *J. Geophys. Res.*, **110**, A12S00, doi:10.1029/2005JA011523.
Gopalswamy, N., Yashiro, S., Michalek, G., Xie, H., Lepping, R. P., Howard, R. A. 2005c, *Geophys. Res. Lett.*, **32(12)**, CiteID L12S09.
Gopalswamy, N., Xie, H., Yashiro, S., Usoskin, I. 2005d, *29th ICRC Conference*, Pune.
Gopalswamy, N., Aguilar-Rodriguez, E., Yashiro, S., Nunes, S., Kaiser, M. L., Howard, R. A. 2005e, *J. Geophys. Res.*, **110**, A12S07, doi:10.1029/2005JA011158.
Gopalswamy, Fleck, B. and Gurman, J. B. 2005f, In the Proceedings of Asia Pacific Regional Conference of IAA "Bringing Space Benefits to the Asia Region", (eds) Rao, M. & Murthy, R. L. N. Astronautical Society of India, Bangalore, in press.
Gosling, J. T., 1993, *J. Geophys. Res.*, **98**, 18937.
Hildner, E. *et al.* 1976, *Solar Phys.*, **48**, 127.
Hansen, R. T., Garcia, C. J., Grognard, R., Sheridan, K. V., 1971, *Proc. ASA*, **2**, 57.
Hirshberg, J., Bame, S. J., Robbins, D. E. 1972, *Solar Phys.*, **23**, 467.
Howard, R. A., Michels, D. J., Sheeley, N. R. Jr., Koomen, M. J. 1982, *ApJ*, **263**, L101.

Hundhausen, A. J. 1999, In: *Many Faces of the Sun* (eds) Strong, K. T., Saba, J. L. R., Haisch, B. M., Springer-Verlag, New York, p. 143.
Kahler, S. W. 2001, *J. Geophys. Res.*, **106**, 20947.
Lara, A., Gopalswamy, N., Caballero-Lopez, R., Yashiro, S., Valdes-Galicia, J. 2005, *ApJ*, **625**, 441.
Lindemann, F. A. 1919, *Phil. Mag.*, **38**, 669.
Lindsay, G., Luhmann, J. G., Russell, C. T., Gosling, J. T. 1999, *J. Geophys. Res.*, **104**, 12515.
Newkirk, G., Hundhausen, A. J., Pizzo, V., 1981, *J. Geophys. Res.*, **86**, 5387.
Payne-Scott, R., Yabsley D. E., Bolton, J. G. 1947, *Nature*, **160**, 256.
Reames, D. V. 1999, *Space Sci. Rev.*, **90**, 413.
Sheeley, N. R., Walters, J. H., Wang, Y.-M., Howard, R. A. 1999, *J. Geophys. Res.*, **109**, A10103.
Srivastava, N., Venkatakrishnan, P. 2004, *J. Geophys. Res.*, **109**, A010103. doi10.1029/2003JA010175.
St. Cyr, O. C. *et al.* 2000, *J. Geophys. Res.*, **105**, 18169.
Tousey, R. 1973, *Space Res.*, **13**, 713.
Tandberg-Hanssen, E. 1995, *The Nature of Solar Prominences*, Kluwer, Dordrecht.
Vourlidas, A., Buzasi, D., Howard, R. A., Esfandiari, E. 2002, In: *Solar variability: from core to outer frontiers* (ed.) Wilson, A., ESA SP-506, Vol. 1., p. 91, ESA Publications, Noordwijk.
Wagner, W. J. 1984, *ARA&A*, **22**, 267.
Webb, D. F., Howard, R. A. 1994, *J. Geophys. Res.*, **99**, 4201.
Webb, D. F., Cliver, E. W., Crooker, N. U., St. Cyr, O. C., Thompson, B. J. 2000, *J. Geophys. Res.*, **105**, 7491.
Yashiro, S., Gopalswamy, N., Michalek, G., St. Cyr, O. C., Plunkett, S. P., Rich, N. B., Howard, R. A. 2004, *J. Geophys. Res.*, **109**, A07105.
Yurchyshyn, V. B., Wang, H., Goode, P. R., Deng, Y. 2001, *Astrophys. J.*, **563**, 381.
Yurchyshyn, V., Hu, C., Abramenko, V. 2004, *Space Weather*, **3**, S08C02.
Yurchyshyn, V., Yashiro, S., Abramenko, V., Wang, H., Gopalswamy, N. 2005, *Astrophys. J.*, **619**, 599.